Journal of Nuclear Materials 390–391 (2009) 10–19

Contents lists available at ScienceDirect

Journal of Nuclear Materials

journal homepage: www.elsevier.com/locate/jnucmat

Power and particle exhaust in tokamaks: Integration of plasma scenarios with plasma facing materials and components

W. Fundamenski

Euratom/UKAEA Fusion Association, Culham Science Centre, Abingdon, OX14 3DB, UK

ARTICLE INFO

PACS:
52.55.-s
52.55.Fa

ABSTRACT

Fusion ignition, on the one hand, and particle and power exhaust, on the other, impose often conflicting criteria on the plasma scenario – the former requiring the plasma to be sufficiently heated, fuelled and confined, the latter the helium ash, impurity ions and the total input + fusion power to be removed without undue damage to the reactor itself, specifically its plasma facing components (PFCs) – necessitating an optimization of the latter to attain the optimum fusion gain for a given reactor design. Foremost among these problems is the issue of power exhaust, including both steady-state and transient heat loads on PFCs. This review examines the various strategies of reducing plasma loads on PFCs at the minimum penalty to the performance of a fusion reactor, specifically ITER, and attempts to quantify the impact of a given PFC limit in terms of the relative change to the fusion gain factor compared to the no-limit value.

1. Introduction: compatibility vs. optimization

By definition, all *exothermal* reactors, including any fusion reactor one may envisage (tokamak, stellerator, etc.), produce both energy and spent reactants, or ash. In order for the reactor to operate in steady-state, (i) fresh fuel must be added at the rate at which it is consumed, (ii) this fuel must be heated, ideally by the reactions themselves, (iii) fuel must be confined, by whatever means are available, for sufficiently long to allow the exothermic processes to continue, (iv) the energy and ash must be removed from the system at the rate at which they are created, (v) the impurities released from the reactor walls during this exhaust process must not inhibit the ignition (burn) of fuel, and (vi) the reactor itself, primarily its walls, must not be damaged by all the exhaust processes. Translating the above to a D-T burning tokamak, conditions (i)–(iii) may be labelled loosely as the *ignition* criteria, and conditions (iv)–(vi) as the *exhaust* criteria. Taken together they constitute the criteria of mutual *compatibility* between the burning plasma and first wall materials/components. Since the latter provide the boundary conditions for the plasma thermodynamic quantities (density, temperature and pressure), they effectively determine the maximum achievable fusion gain, $Q = P_{fus}/P_{heat}$, for a given reactor design (RD), by which we mean a set of hardware including magnetic coils, heating, fuelling and current drive systems, vacuum vessel and mechanical support, cooling and pumping systems and last, but not least, the plasma facing components (PFCs), i.e. the first wall armour against plasma fluxes. This relation may be expressed as

$$Q = Q(\mathrm{PS}, \mathrm{RD}), \tag{1}$$

$$Q_{max} = Q_{max}(\mathrm{RD}) = \text{maximum } Q(\mathrm{PS}, \mathrm{RD}) \text{ over all PS}, \tag{2}$$

where *plasma scenario* (PS) refers to a combination of plasma shape, magnetic field, current profile, heating and fuelling methods, etc, i.e. to the way in which the given reactor design is utilised within each plasma discharge. Thus, the issue of *compatibility* or *integration* between the ignition and exhaust criteria, and specifically between plasma scenarios and PFCs, is really one of *optimization* of the PS for a given RD with respect to Q; note that the very terms 'compatibility' and 'integration' reflect the historical disconnect between the tasks of investigating, on the one hand, the plasma equilibrium, stability and transport, and on the other, its particle and power exhaust properties, a disconnect which is of course absent in a real plasma. Since the fusion power density is roughly proportional to the square of the central fuel ion plasma pressure, $P_{fus}/V \sim n_D n_T \langle \sigma v \rangle_{fus} \sim p_i^2$, and the maximum electron density is given roughly by the Greenwald density [20], $n_{GW} \sim I_p/\pi a^2$, where I_p is the plasma current and a the minor radius, this optimization amounts to maximizing the ion temperature, T_i, and minimizing the effective charge, Z_{eff}, in the centre of the plasma column. In the absence of internal transport barriers, e.g. in the inductive or baseline tokamak plasma scenario, the ion temperature gradient (ITG) is set by the threshold for the ITG drift-wave turbulence [15]. Hence, the central ion temperature is a linear function of the edge, or *pedestal*, temperature, T_{ped}, e.g. in ITER, it is predicted that

E-mail address: wojtek.fundamenski@jet.uk

0022-3115/$ - see front matter © 2009 W. Fundamenski. Published by Elsevier B.V. All rights reserved.
doi:10.1016/j.jnucmat.2009.01.038

$T_{ped} \sim 4$ keV is necessary to achieve the desired fusion gain factor, $Q \sim 10$ [24]. Whether such high edge plasma temperatures are compatible with the desired lifetime of the divertor and limiter PFCs remains a matter of research and debate in the fusion plasma community. The key aim of this contribution is to shed light on this very point by reviewing the current status of our understanding of particle and power exhaust in tokamaks, focussing primarily on the latter, and its implications for both steady-state and transient heat loads on divertor and limiter PFCs; an attempt is made to avoid repetition of material presented in a recent reviews of this subject [22,23,36,51].

To illustrate the problem, let us consider the global power balance in ITER assuming 40 MW of auxiliary heating power and $Q = 10$. Since 80% of the D–T fusion power is released in the form of neutrons, this leaves 40 + 80 = 120 MW transferred to the plasma. Of this, let us assume that some substantial fraction, say $f_{rad}^{core} \sim 50\%$, can be radiated in the core of the plasma by bremstrahlung, synchrotron and line radiation, so that only $P_{SOL} = 60$ MW crosses the separatrix (this fraction is determined by the requirement of accessing and maintaining the H-mode, with $P_{SOL}/P_{LH} > 1.5$ desirable; the threshold power for the L–H transition is estimated as $P_{LH} \sim 40$–50 MW in ITER according to a rough scaling of $q_{perp}^{L-H} \propto n_e^{0.64} B_t^{0.78}$ [24]). Of this, we expect ~2/3, or 40 MW, to be exhausted between ELMs, and ~1/3, or 20 MW, by the ELMs themselves [38]. Assuming an asymmetry of 2:1 in favour of the outer target for the total energy, and 1:2 for the ELM energy, see Section 3, we expect the power to the inner and outer divertor legs between and during the ELMs to be: inner = (6,14) MW and outer = (34,6) MW. Estimating the respective plasma wetted areas as $A = 2\pi R_{div} \times \lambda_q \times FX_{eff}$, where R_{div} is the major radius at the divertor, λ_q is the integral deposited power width mapped to the outer mid plane, and FX_{eff} is the effective flux expansion (ratio of distances along the target and outer mid plane), we find $A_{in} \sim 2\pi \times 5\ \text{m} \times 4\ \text{mm} \times 10 \sim 1.2\ \text{m}^2$ and $A_{out} \sim 2\pi \times 6\ \text{m} \times 4\ \text{mm} \times 10 \sim 1.5\ \text{m}^2$. The maximum steady-state and transient heat loads for divertor PFCs (irrespective of whether these are made from CFC or W) have been imposed at ~10 MW/m^2 and 0.5 MJ/m^2 in 250 μs to peak, respectively. This implies that of the 40 MW reaching the outer divertor volume, at least 25 MW, or $f_{rad}^{outer} \sim 60\%$, has to be removed by volumetric losses (charge exchange, elastic scattering and line radiation) in the divertor itself. Similarly, the transient limit implies a minimum ELM frequency of $f_{ELM}^{min} \sim 14\ \text{MW}/(1.2\ \text{m}^2 \times 0.5\ \text{MJ/m}^2) \sim 23$ Hz and a maximum ELM size of $\Delta W^{max} \sim 3/2 \times 1.2\ \text{m}^2 \times 0.5\ \text{MJ/m}^2 \sim 0.9$ MJ, or less than 1% of the pedestal stored energy, $W_{ped} \sim 1/3 \times W_{dia} \sim 133$ MJ, where $W_{ped} = 3/2 \times n_{ped}(T_{i,ped} + T_{e,ped})V$. At present, it is not clear whether the above factors ($f_{rad}^{core}, f_{rad}^{outer}, f_{ELM}^{min}$) can be achieved while maintaining $Q \sim 10$. Therefore, one should repeat the calculation in the opposite direction, starting from the specified PFC heat load limits and estimate the resulting $Q(PFC)$ value for a given set of modelling assumptions (such a calculation can be done with various degrees of sophistication starting from the simple power balance above and ending with a fully integrated core/edge/SOL transport model [64]). The impact of any given PFC limit on the reactor performance can then be quantified as

$$\zeta_P FC = \zeta(PFC) = \Delta Q_{max}(PFC)/Q_{max,0} = 1 - Q_{max}(PFC)/Q_{max,0}, \qquad (3)$$

where $Q_{max}(PFC)$ is the maximum fusion gain factor for a specified PFC limit, i.e. Eq. (2) with PFC in place of RD, and $Q_{max,0} = Q(no\ PFC\ limits)$ the same factor without any limit on PFC plasma loads (or some previously chosen reference limit value). Note that one can recast (3) in terms of a confinement degradation by estimating $Q \sim p\tau E \sim (f_{GW} H_{98})^{\alpha}$ so that

$$\zeta_{PFC} \sim 1 - [f_{GW}(PFC) H_{98}(PFC)/f_{GW,0} H_{98,0}]^{\alpha}, \quad \alpha \sim 2\text{–}3, \qquad (4)$$

where $f_{GW} = n_e/n_{GW}$ is density normalised by n_{GW} and H_{98} is the energy confinement time normalised by the ITER98(y,2) scaling (the values required by the ITER reference scenario are $f_{GW} \sim 0.85$ and $H_{98} \sim 1$). Similar impact factors could be obtained for other limits, e.g. tritium retention, discussed in [37]. Finally, an alternative measure of reactor performance, e.g. bootstrap fraction, neutron fluence, cost, could be used instead of Q to defined the impact factor.

2. Steady-state particle and power exhaust

2.1. Limiter vs. divertor exhaust

The exhaust properties of a magnetised fusion plasma are determined largely by (a) the region of closed field lines inside of, but in close vicinity to, the last closed flux surface (LCFS), usually referred to simply as the 'edge' plasma, and (b) the boundary plasma layer, or Scrape-Off Layer (SOL), defined as the region of open field lines beyond the LCFS. There are three types of SOL: (i) the *limiter* SOL formed by solid object (a limiter) protruding from the wall, (ii) the *divertor* SOL formed by creating magnetic null, or X-point, with additional poloidal field coils, and thereby diverting the plasma into the divertor volume, and (iii) the *ergodic* SOL, formed by perturbing the edge magnetic field until its lines of force are ergodized into chaotic volumes; all three SOL-configurations have their merits and each has been explored experimentally in several tokamaks [60]. However, it is the divertor configuration which has emerged as the leading candidate for satisfying the exhaust criteria outlined in Section 1, with minimal penalty to the fusion gain. The main advantage of the divertor over the limiter SOL can be traced to two facts: (i) the physical sputtering yield increases with projectile energy while decreasing with the target atomic mass [7], and (ii) by moving the PFC away from the LCFS, it allows localized plasma recycling in the divertor SOL, thereby attaining a colder, denser plasma compared to the limiter SOL [60]. This improves particle compression and exhaust, and reduces the plasma temperature, erosion yields and net impurity sources. Moreover, by distancing these sources away from the LCFS, it reduces their penetration into the core plasma, hence improving plasma purity and increasing the fusion power.

In all three cases, and indeed for any combination of these, the radial width of the SOL is determined by competition between parallel and perpendicular transport. Parallel transport is generally well understood and can be described to a fair accuracy by either the 1-D Fokker–Planck equation or the Braginskii equations (aside from specific kinetic effects in non-local heat flow), under low and high collisionality conditions, respectively. In contrast, perpendicular (radial) transport is generally governed by turbulent advection, whose mechanism and dynamics has for a long time remained elusive, acquiring the fatalistic label 'anomalous', i.e. abnormal, irregular, not understood. Since our ability to predict the steady-state plasma loads on PFCs (divertor or limiter tiles) reflects the degree to which we can understand and model edge/SOL turbulence, it is encouraging to find that significant progress has been recently made in this domain, with the governing mechanisms having been identified and predictive capability coming into view. Indeed, somewhat ironically, it now appears that that it is the absence, rather then presence of edge/SOL turbulence, which may be properly described as anomalous, since the formation of the edge transport barrier (ETB) and the related high confinement (H-mode) regime are still not properly understood and remain the chief source of uncertainty in all aspects of tokamak plasma behaviour, including its exhaust properties. Indeed, although one might expect turbulence reduction due to poloidal and toroidal flow shear and/or magnetic shear in the X-point geometry, the observed bifurcation from low to high confinement has yet to be quantitatively reproduced [4].

2.2. L-mode exhaust physics

Before tackling the issue of plasma exhaust in H-mode, let us briefly review the progress in L-mode exhaust physics, i.e. in the understanding of edge/SOL turbulence. It is now widely recognised that this turbulence originates in the edge region, where it is driven by a combination of drift-wave, or rather drift-Alfven wave, and interchange dynamics [43,58]. These reduce to resistive-MHD (resistive ballooning) dynamics with increasing collisionality, and to ideal MHD (ideal ballooning) dynamics with increasing pressure gradient, i.e., there is a continuity between the mechanisms determining edge plasma (in)stability and transport. Since drift-waves are strongly damped in the region of open field lines, turbulent motions in the SOL are dominated by interchange dynamics, supplemented by parallel losses and sheath dissipation at the plasma–solid interface [58]. Overall, the free energy driving edge/SOL turbulence is provided by radial pressure gradients, which build up together with poloidal ExB flow shear during relatively long, quiescent periods. These are sporadically interrupted by formation and ejection of plasma filaments (blobs) into the SOL, which advect mass, momentum and energy into the far-SOL, defined as the SOL region beyond one-two power widths away from the LCFS, while draining to the divertor [3]. This highly intermittent nature of SOL transport results in strong fluctuations in far-SOL quantities, which for most of the time represent a cool and rarefied plasma background, which is occasionally punctuated by relatively dense and hot plasma filaments. This has two important consequences. First, the local radial fluxes are not related to the local gradients, as assumed in the diffusive approximation, i.e. Fick's law, and most quasi-linear approaches. Second, the mean field approximation, which follows the evolution of mean quantities, $\langle A\rangle$, and hence relies on the smallness of fluctuating quantities, $\delta A = A - \langle A\rangle$, is no longer valid, e.g. if the temperature and density are 1 eV and 1e18 m^{-3} for nine time units, followed by 10 eV and 1e19 for one time unit, it is not helpful to simply cite the mean values of $\langle T\rangle = 1.9$ eV and $\langle n\rangle = 1.9e18$ m^{-3}, since their product, $\langle n\rangle\langle T\rangle = 3.61e18$ eV m^{-3} is much smaller than the mean pressure, $\langle p\rangle = \langle nT\rangle = 1.09e19$ eV m^{-3}; such discrepancies become even larger when considering higher order moments, e.g. the heat flux. Since the mean-field approximation, applied to the Braginskii equations, is the basis of most edge transport codes, e.g. SOLPS [57], EDGE2D [52], UEDGE [50], etc., it calls into question the accuracy of these tools, and argues strongly for the development of global edge turbulence codes, following total, rather than simply mean or fluctuating, quantities. Indeed, the above limitation is the likely explanation of the inability of such codes to reproduce the SOL radial electric field in relatively simple L-mode plasmas [5].

The above findings are supported by a range of experimental [3,70] and numerical [43,58] studies. However, the recent experiments performed on the TCV tokamak deserve a special mention, as they offer perhaps the clearest insight yet into the nature of SOL turbulence. The experiments, described in [17], consist of two separate scans in otherwise identical L-mode plasmas: the first in plasma density, the second in the plasma current, both of which (independently) vary the separatrix collisionality, $\nu^* \propto \alpha n L_{\parallel}/T^2$. As was previously observed on many tokamaks, most notably Alcator C-mod [32], the SOL mean density profile (measured near the outer mid-plane at high frequency with a reciprocating Langmuir probe assembly) was found to broaden with increasing ν^*, especially the far-SOL, and to be characterized by large density fluctuations, increasing with radius from $\delta n/\langle n\rangle \approx 0.25$ in the near-SOL to $\approx$0.75 in the far-SOL, Fig. 1. The probability distribution function (PDF) of density fluctuations in the far-SOL was found to be universal and highly intermittent. The radial plasma flux, $\Gamma_r = \langle n v_r\rangle$, was also found to increase with collisionality, while the effective radial

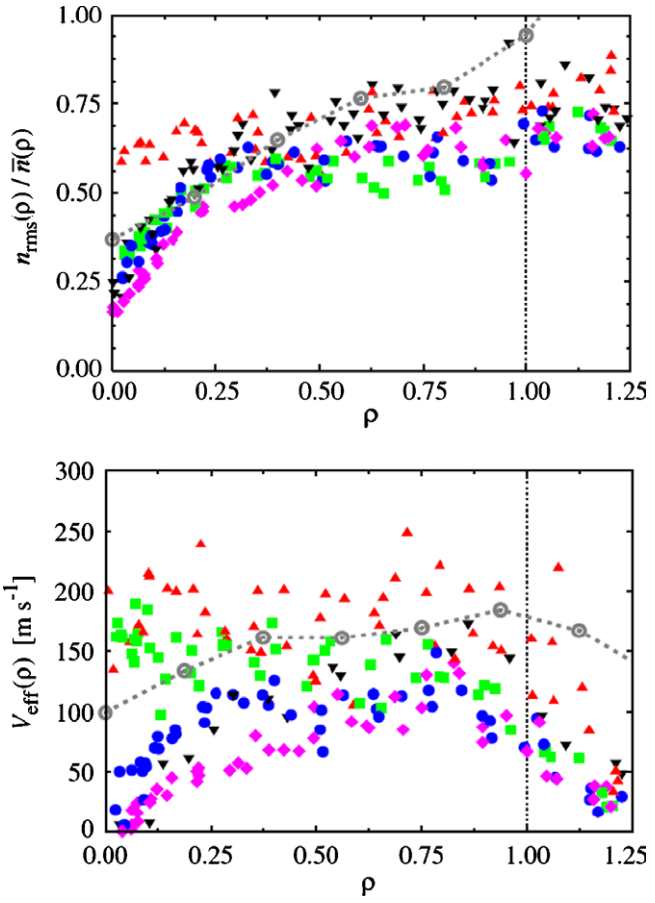

Fig. 1. Radial SOL profiles ($\rho = 0$ represents the separatrix) of relative density fluctuations (top) and effective velocities as measured in TCV for different values of the separatrix density; the dotted line shows the results of an ESEL turbulence simulation. Reproduced from [16].

velocity, defined as $v_{eff} = \Gamma_n/\langle n\rangle$, increased gradually with radius, approaching a flat profile at high ν^*, Fig. 1; similar increase of v_{eff} with radius was observed on many tokamaks [36]. As with the density, the PDF of velocity fluctuations in the far-SOL was again universal and highly intermittent. The temporal pulse shape of the plasma 'blob' recorded by the probe in the far-SOL revealed a sharp leading front and a long trailing wake, suggesting a highly dispersive radial motion.

All the above observations, i.e. all the measured radial profiles, can be quite accurately reproduced using an edge-SOL electrostatic (ESEL) turbulence simulation local to the outer mid-plane, yet including parallel losses of particles, momentum and energy in the SOL region, Fig. 1. This is especially impressive since the code involves no free parameters, providing strong evidence for the dominance of interchange dynamics in determining SOL turbulence.

The observed collisionality dependence may be explained as follows [16]: The equation of motion of plasma filaments (blobs) is determined by charge conservation,

$$\nabla \cdot \mathbf{J} = \nabla \cdot (\mathbf{J}_p + \mathbf{J}_* + \mathbf{J}_\parallel) = 0 \tag{5}$$

expressing the balance between the divergences of the polarization, diamagnetic and parallel currents, which represent the ion inertia (vorticity), interchange (curvature + pressure) drive and parallel damping. At low collisionality, in a so-called sheath-limited regime, the parallel current is determined by the electrostatic sheath at the solid targets, which tends to reduce the interchange drive. As the collisionality increases, the plasma filaments become electrically

isolated from this sheath, making the interchange drive more effective, and thus increasing the radial effective velocity. This explains why the ESEL code without the sheath dissipative damping has overestimated, by roughly a factor of 3, $\nu_{\rm eff}$ and $\lambda_{\rm n}$ on JET, whose SOL is far less collisional than that in typical TCV plasmas. It also suggests a route for both a quantitative and physics based prediction of steady plasma loads on main chamber PFCs in L-mode discharges in ITER.

2.3. H-mode exhaust physics

We next consider plasma exhaust in ELMy H-mode plasmas, which can be divided in the inter-ELM and ELM phases. As we will treat the effects of ELMs separately in the following section, let us first focus on the inter-ELM phase, or alternatively, on the time-averaged exhaust, as we are particularly interested in the time-averaged plasma loads on divertor PFCs. These were measured in JET in a variety of ELMy H-mode plasmas for a variety of fields, currents, heating power and ion species [11]. With low fuelling, i.e. under natural density conditions, the integral power width at the outer target, which receives most of the steady-state energy (the inner:outer asymmetry being ~1:2–2.5, see Section 3) was found to scale as

$$\lambda_q \propto A^{\alpha} Z^{\beta} B_T^{-1.03} q_{95}^{0.6} P_{div}^{-0.41} n_u^{0.25}, \alpha + \beta \approx 1.04 \quad (6)$$

i.e. to decrease with toroidal field, B_T, plasma current, $I_p \propto {q_{95}}^{-1}$, and power to the (outer) divertor target, P_{div}. The smallest value was ~5 mm mapped to the outer mid-plane, or roughly one ion poloidal gyro-radius at the mid-pedestal temperature, Fig. 2; this narrow inter-ELM profile was recently confirmed by a high resolution IR system. The measured scaling is best explained by a collisional (neoclassical) ion conduction, which is consistent with the partial extension of the ETB into the near-SOL, and thus a reduction of the turbulent transport down to ion collisional levels. This result, which was initially obtained based on two point model estimates of the SOL, was recently confirmed with multi-fluid (EDGE2D) simulations, with variable transport coefficients [31]. It is on the basis of this analysis that one may estimate the ITER power width as ~3.5–4.5 mm, and thus obtain the plasma wetted area predictions cited in Section 1. It is worth noting that a similar value has been estimated using a purely empirical extrapolation based on measurements of power widths on various tokamaks [36].

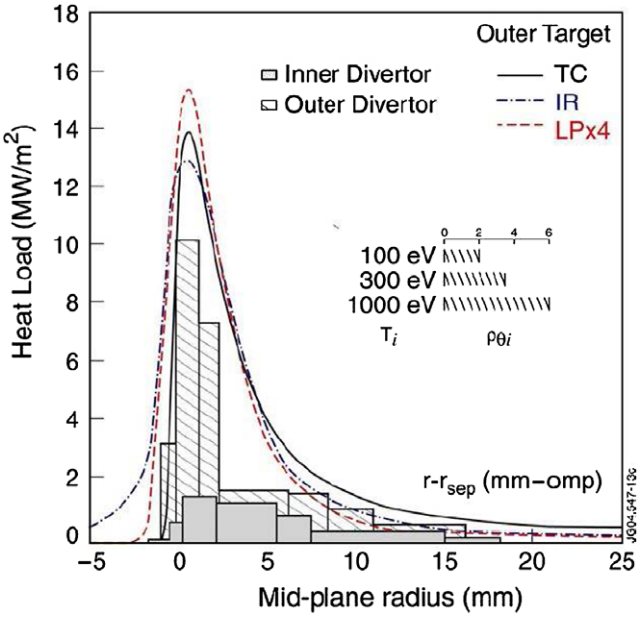

Fig. 2. Outer target heat load profiles, mapped to the outer mid-plane, in a typical, natural density ELMy H-mode discharge on JET (2.5 MA, 2.5 T, 16 MW NBI) as measured by the thermocouple method, infra-red thermography and Langmuir probes. Reproduced from [14].

It is worth stressing that the above value represents the power width at the entrances into the ITER divertor, which being much more closed than the divertor on JET – and indeed most of today's tokamaks – has a capacity to broaden the power profile substantially. To quantify this effect one has to consider the various divertor/SOL operating regimes [60]. We have already mentioned the sheath limited, or low recycling, regime in which both density and temperature are roughly uniform along the field line from the upstream (u) to the target (t) locations: $n_t \sim n_u$, $T_t \sim T_u$. At higher collisionality, the divertor enters the conduction limited, or high recycling, regime in which the pressure remains uniform, but the temperature and density vary along the field line in accordance with the electron heat conduction equation, so that $n_t \propto n_u^3$, $T_t \propto n_u^{-2}$, resulting in increasing compression and cooling of the target plasma compared to the upstream SOL.

2.4. Divertor plasma detachment

At still higher collisionality, the divertor enters the charge–exchange limited, or (partially) detached regime, characterized by loss of plasma pressure and energy by interaction with neutrals and by a reduction (roll-over) of the density at, and plasma particle and heat fluxes to, the divertor target; the term 'detachment' derives its name from the concurrent movement of the ionisation and radiation fronts away from target. Since momentum is removed by charge exchange and elastic collisions with neutrals in the divertor volume, increased neutral density and hence divertor 'closure' is found to facilitate detachment, e.g. it is easier to achieve on vertical compared to horizontal targets; similarly, energy is removed by the above processes, plus hydrogenic and impurity line radiation, so that impurity seeding also acts as a catalyst for divertor detachment.

Since detachment is achieved by each neutral experiencing many charge exchange collisions before being ionised, it requires the divertor plasma to be sufficiently cold, typically ~5 eV for deuterium (the exact value is a function of divertor 'closure'). In its later stages, i.e. at the highest densities, it is accompanied and assisted by volumetric recombination, which removes plasma species and can eradicate plasma–surface (although not plasma-neutral) interaction at the divertor target altogether; indeed, divertor neutral pressure increases during the onset of detachment, later saturating and/or decreasing as the ionisation front moves away from target. In short, detachment is beneficial in both (i) reducing the steady state heat loads, by transferring part of the power entering the divertor from the plasma to the neutrals, and hence distributing it over a larger PFC area, and (ii) cooling the divertor plasma and hence reducing the impurity source due to physical sputtering and the impurity influx to the core plasma. The second item is especially important if the divertor targets are made from tungsten (envisioned for the D–T phase of ITER and is the most likely PFC material for DEMO), which has a physical sputtering threshold of ~200 eV (impact energy) for deuterium. Since this impact energy is roughly $2T_i + 3ZT_e$, it means that W sputtering by D vanishes when $T_e \sim T_i < 40$ eV; for higher Z impurities, a further reduction of T_e is required, e.g. $T_e \sim T_i < 6$ eV for $Z = 10$, corresponding to the T_e needed for detachment.

Consistent with the larger average power flow into the outer divertor volume (for normal field direction, when $B \times \nabla B$ points down, i.e. towards the divertor), the inner target typically detaches earlier, i.e. at lower upstream density, than the outer target. This asymmetry is enhanced by guiding centre (mainly $E \times B$) drifts and diamagnetic flows which tend to increase the power flow to

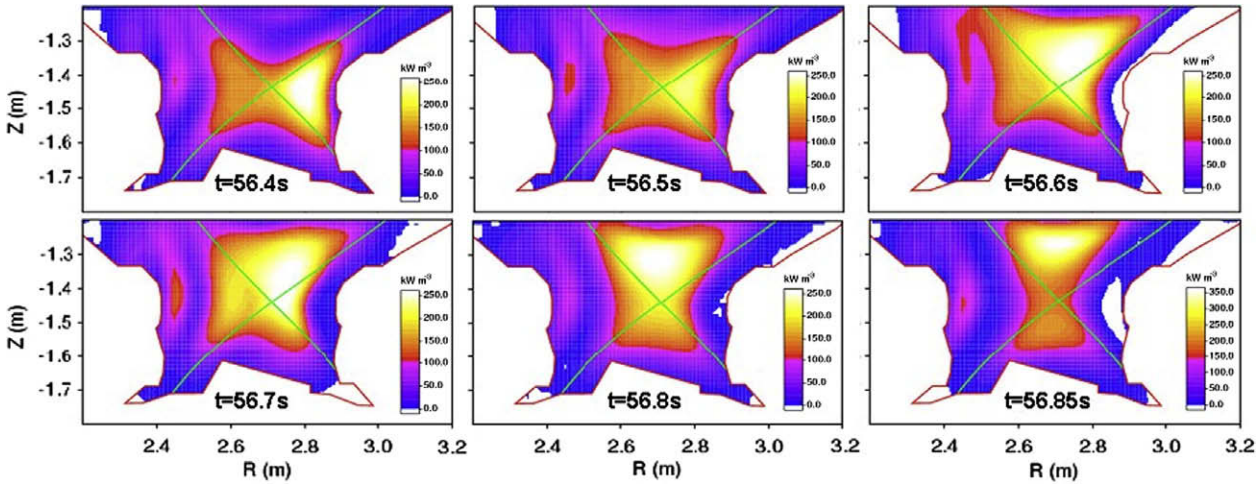

Fig. 3. Poloidal profiles of radiated power (as measure by bolometry) during a density scan on JET, corresponding to outer target divertor detachment and the formation of an X-point MARFE. Reproduced from [21] [53,54].

the outer divertor for this field orientation, making the inner divertor leg colder and denser at a given upstream density, and hence easier to detach (see Section 3). As a result, detaching the outer divertor plasma during the inter-ELM phase can be viewed as one of the main exhaust challenges for any tokamak fusion reactor, including ITER. The word 'challenge' is chosen carefully, since complete detachment of the outer target leads to a radiation limited divertor regime, accompanied by the movement of the radiation front from the divertor volume into the X-point region, i.e. by the formation of a so-called X-point MARFE, Fig. 3. This results in strong cooling of the edge plasma and a reduction of pedestal pressure by roughly a factor of 2 in ELMy H-mode, Fig. 4 [2]; since $W_{ped} \sim W/3$, this is equivalent to a ~15–20% drop in the normalised energy confinement factor, $H_{98} = \tau_E/\tau_{E98y}$. This is typically accompanied by a Type-I to Type-III ELM transition [53,54] which appears to be determined by a critical temperature and/or resistivity, rather than a critical collisionality, see Section 3.

At still higher densities the radiation shifts to the inner half of the torus (a wall MARFE) and eventually terminates the discharge via a thermal collapse (radiative disruption). Although the details of this maximum density, or *density limit*, are still under debate [20], it can be approximated to a fair accuracy by the Greenwald density, $n_{GW} \sim I_p/\pi a^2$, recall Section 1. It is suggestive that $n_{GW}/I_p \propto nL_{||} \propto T^2\nu^*$ defines some critical collisionality for a given edge temperature. Since the (turbulent) radial transport in the SOL increases with ν^*, as is manifest in the observed broadening of the upstream SOL profiles, this suggests some link between main chamber recycling and the density limit.

Our predictive capability relating to detachment is at present still limited. Although most of the above tendencies can be reproduced by 2D multi-fluid/M-C codes, these codes are not able to reproduce all the measurements simultaneously, even under relatively simple Ohmic and L-mode conditions [67]. Possible reasons for these discrepancies, i.e. the physics missing from these codes, include:

(i) SOL plasma turbulence involves strong thermodynamic perturbations, e.g. $\delta n/\langle n\rangle \sim 1$. Hence, the mean field formulation on which the 2D codes are based may be inaccurate, e.g. $\langle nT\rangle = \langle n\rangle\langle T\rangle + \langle \delta n \delta T\rangle$, with the second terms no longer small. Similarly, the turbulent closure schemes which are typically used, e.g. Prandl mixing length approximation with $D_\perp \sim$ const, may also generate large errors. Finally, the problem becomes 3-D rather than 2-D, as the axisymmetry is broken by turbulent plasma filaments;

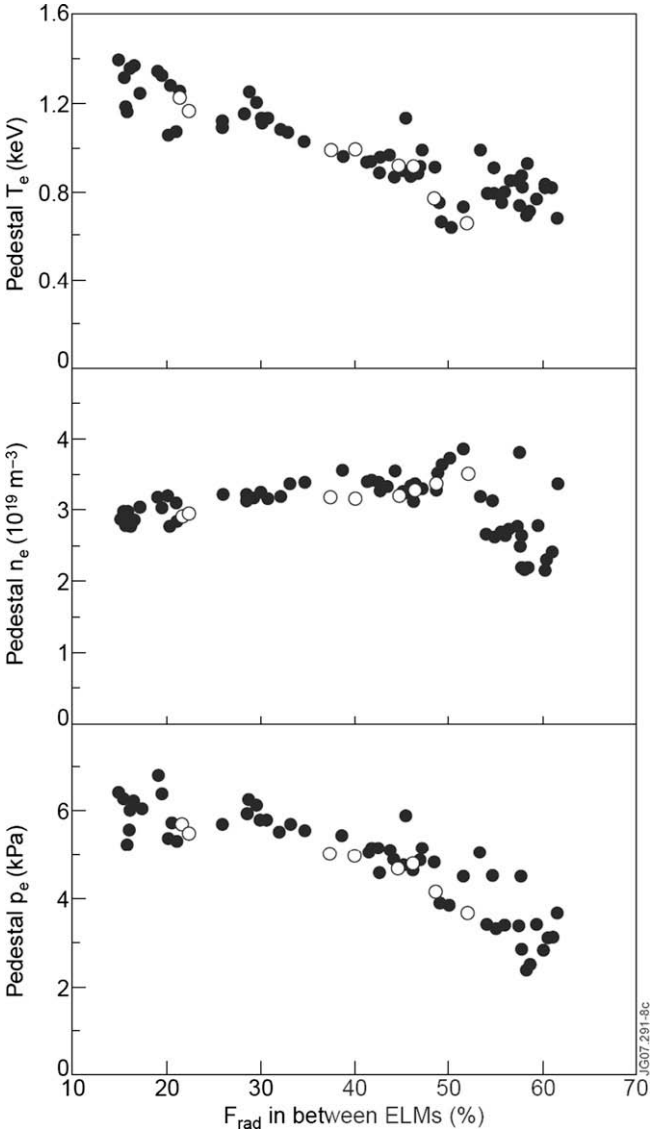

Fig. 4. Variation of pedestal electron temperature, density and pressure with inter-ELM radiative fraction in a radiative seeding scan in JET. Reproduced from [2].

(ii) Kinetic effects (non-local heat transport) become important in detachment fronts. Spitzer–Harm (S–H) closure for heat flux and viscosity become invalid, while the heat flux limit corrections become inadequate, since the heat flux can actually exceed the S–H value when hot electrons stream into a cold region [65,66,71];
(iii) other possible source of error include neutral, photon and impurity effects. For instance, under dense divertor conditions, neutrals become fluid-like and most likely turbulent, while photon transport becomes opaque in certain lines, e.g. Lyman alpha.

2.5. Power exhaust by radiative impurities

Above we considered what happens to the divertor target particle and heat loads in a density, or fuelling, scan, which increases $\nu^* \propto nL_{\|}/T^2$ primarily via the edge density. Let us next consider what happens in a radiation, or extrinsic impurity seeding, scan, which increases ν^* primarily by reducing the edge temperature. As one might expect, the radiative cooling of the edge plasma reduces both W_{ped} and H_{98}. Thus, both fuelling and seeding can have determintal effects on global energy confinement, i.e. H_{98} decreases when either the Greenwald fraction ($f_{GW} = n/n_{GW}$) or the radiative fraction ($f_{rad} = P_{rad}/P_{heat}$) exceed values of ~0.7–0.8.

The additional hazard associated with impurity seeding is the possibility of increased impurity concentration, and hence, of the effective charge, Z_{eff}, in the core plasma, with a detrimental effect on core fuel density and fusion gain factor. Needless to say, impurity transport in the edge/SOL and core region fully deserves the label 'anomalous': it is one of the least understood processes in fusion plasmas, involving a combination of turbulent and collisional (neoclassical) processes. While some attempts have been made at predicting the impurity concentration in the core by measuring the 'screening' of the edge/SOL plasma to a known extrinsic impurity sources, such attempts are largely limited to low-Z impurities and specific divertor/SOL conditions [61]. An even simpler approach relies on an empirical scaling of $Z_{eff} - 1$, which is found to increase roughly linearly with the radiative heat flux ($P_{rad}/\pi a^2$) and decrease roughly as the square of line averaged electron density [40,63]. A straight forward application of this scaling to the reference scenario in ITER (Ar seeding, 75% radiation) predicts $Z_{eff} \sim 1.7$, or ~1.9 based on a revised scaling [72], is consistent with integrated modelling under the assumption of no anomalous impurity pinch [68] (although this assumption is not supported by recent experimental data [19]).

An additional cause for concern is the tendency of high-Z impurities to accumulate towards the centre of the discharge under the influence of purely collisional (neoclassical) transport. Since, to a fair approximation, this situation is achieved within the internal transport barrier (ITB), it is not surprising to find central peaking of high-Z impurity densities, e.g. Ar, in discharges with strong ITBs [62]. This problem is particularly acute for advanced tokamak (AT) scenarios, which rely on the ITB to recover the stored energy lost by operating at higher q_{95} (lower I_p), than the baseline scenario ($q_{95} \sim 5$ in AT vs. ~3 in baseline scenario) [1].

3. Transient particle and power exhaust

3.1. Edge transport barrier and edge localized modes

The H-mode confinement regime relies on the presence of the edge transport barrier (ETB) which more than doubles the average edge plasma pressure compared to the L-mode level, i.e. $W^H \sim 2W^L$ so that $\tau_E^H \sim 2\tau EL$. However, the ETB is periodically destroyed by edge localized instabilities, or modes (ELMs), which lead to intense plasma heat loads on the divertor, and to a lesser extend on the main chamber PFCs. The ELM may be divided into three stages [11]: (i) the growth stage in which the linear instability (and ideal/resistive MHD mode) forms ~ 10–20 flute-like ripples in pedestal quantities, (ii) the transport stage, in which these develop into ~10–20 filaments during the non-linear phase of the instability, and (iii) the exhaust stage in which the filaments move outward, driven by interchange (curvature + pressure) forces, while draining to the divertor targets. ELM observations in tokamaks have been reviewed on several occasions, most recently in [13,27,30,33,45], while its filamentary nature is also well documented [8,13,28].

The result of the ELM is a partial collapse, or erosion, of the pedestal pressure, Δp, which can be divided into a density drop, Δn, associated with 'convective' losses, and a temperature drop, ΔT, associated with 'conductive' losses. The relative pressure drop, $\Delta p/p$, or $\Delta W/W_{ped}$ as it is more commonly expressed, is found to decrease strongly with the pedestal collisionality [33,38]. Moreover, this reduction is primarily due to the reduction of the conductive component, $\Delta T/T \sim \Delta W/W_{ped}$, so that sufficiently small ELMs are dominantly convective, i.e. dominated by density losses.

3.2. ELM plasma loads on divertor PFCs

As with the steady-state power loads, the energy released during the ELM is conveyed primarily to the divertor targets with little broadening of the integral power width (see discussion of main chamber loads below). However, unlike the steady-state power, which is deposited mostly on the outer target (with an inner:outer asymmetry of ~1:2–2.5), the ELM energy is deposited mostly on the inner target (with an inner:outer asymmetry of ~2:1) [8,48]. At present, the reason for these opposite in-out energy asymmetries has not been fully identified. However, a plausible explanation, which emerges based on a number of recent studies may be phrased thus:

It is clear that the radial electric field in the edge and SOL regions points in opposite directions, due to an electric potential well near the separatrix. With the normal magnetic field direction, the electric drift in the SOL points increases the convective energy flow to the outer target. In contrast, the electric drift in the edge region increases the convective energy flow to the inner target. Finally, parallel flows tend to convect the energy equally towards both targets. However, the parallel flow of ions on circulating orbits, which has an effective poloidal flow component, would tend to increase the energy deposited on the target facing towards this flow, since the parallel ion momentum would be roughly preserved as the ELM filaments connect to the divertor targets. This would suggest a link between net poloidal plasma rotation as the ultimate origin of the inner:outer ELM energy asymmetry [8].

This hypothesis is given further credence by examining the parallel transport of the ELM energy. Infra-red thermography measurements at both AUG and JET, indicate that the ELM heat load at both the divertor targets can be explained by arrival of free-streaming ions originating from an initially Maxwellian velocity distribution characterized by a mid-pedestal ion temperature [8,11],

$$P^{ELM}(t)\tau_{\|}/E^{ELM} = \frac{2}{3\sqrt{\pi}}[1+x^2]x^2 e^{-(x-M)^2}, \tag{7}$$

where $x = v_{cr}/v_{Ti} = L_{\|}/tv_{Ti} = \tau_{\|}/t$ is a normalised critical velocity, $\tau_{\|} = L_{\|}/v_{Ti}$ is the characteristic loss time to the target, and $M = u_{\|}/v_{Ti}$ is the Mach number of the parallel projection of the poloidal ion flow in the filament – clearly it is the net poloidal flow contributes to inner:outer asymmetry – with positive value indicating flow towards the target; note that Eq. (7) is a modified version of

the one drived in [11], extended for a non-stagnant initial Maxwellian, i.e for a non-zero M (this expression is in fair agreement with kinetic modelling of the ELM pulse [65,66]). In the presence of both ExB and parallel flows, both of which contribute to the net poloidal flow velocity, $u_P \approx v_E + (B_P/B_T)v_{||}$, its parallel projection becomes $u_{||} = u_P(B_T/B_P) \approx v_E(B_T/B_P) + v_{||}$. Evidently, the ELM energy deposition is symmetric for $M = 0$. However, only a small Mach number towards the inner target, $M \sim 0.2$, is needed to account for the observed inner:outer energy asymmetry of ~2:1 [8]. Experiments are currently planned to resolve the relative contributions of *ExB* drifts and parallel flows to this effective poloidal velocity.

3.3. Maximum ELM size imposed by divertor PFC limits

Returning to the issue of the ELM size, we note that the best estimates of core energy transport predict that the attainment of a fusion gain factor of $Q \sim 10$ in ITER requires a pedestal temperature of $T_{ped} \sim 4$ keV assuming a line average Greenwald density [24]. The corresponding collisionality, $\nu^* \sim 0.06$, would predict a relative ELM size of $\Delta W/W_{ped} \sim 0.2$ or ~25 MJ [38]. Assuming the same wetted area as for the inter-ELM profile, and an inner:outer asymmetry of 2:1, this leads to a transient heat load of ~15 MJ/m^2, with a peak after ~250 μs. This value is well in excess of the transient heat load limits (in ~250 μs) of ~0.5 MJ/m^2 adopted by ITER; the value was chosen based on cyclical plasma gun tests of actual PFC components (interestingly, surface failure was observed at similar values of energy heat loads for both *W* and CFC clad components, although the mode of failure was grossly different [35]; this is possible linked to the similar binding energies of surface atoms, ~8 eV, and similar heat diffusivities, in both armour materials) [69]. Accepting this limit, the maximum allowable ELM size in ITER is estimated as $\sim 0.5\ \mathrm{MJ/m^2} \times 1.2\ \mathrm{m^2} \times 1.5 \sim 0.9$ MJ, or $\Delta W/W_{ped} < 0.01$, i.e. more than a factor of ~20 smaller than the 'natural' ELM size value based on the empirical collisionality scaling [38].

There are of course some caveats in this prediction, e.g. the heat pulse shape used in the plasma gun test differs somewhat from that expected for the ITER ELM, with ~40% of the energy arriving before the peak in the former case, compared to ~20% in the latter. However, while this may relax the limit by up to a factor of two, this is more than offset by the fact that not all ELMs are equal. Indeed, recent studies indicate that the PDF of ELM amplitudes is highly intermittent [38]. Since large ELMs cause the most damage to the PFCs, it may be necessary to ensure that the average (mean) ELM size is well below the threshold value.

3.4. ELM plasma loads on main chamber PFCs

Before discussing the various methods for reducing the ELM size, let us consider the ELM heat loads to the main chamber wall, which are a result of the ELM filament impact. The fraction of ELM energy deposited on the wall for a given ELM size and separatrix-to-wall distance can be reasonably well described by a so-called parallel loss model of ELM exhaust [11]. This model describes the radial motion of the pedestal plasma as an effective filament, moving with some mean radial velocity (which must be obtained from experiment) and subject to parallel losses to the divertor tiles. The filament density and temperature are evolved using the fluid approximation, which although clearly not valid in the initial phase of the ELM (recall the discussion of Maxwellian free-streaming above), is more appropriate to the latter, collisional phase of the ELM. Moreover it does explain some basic features of ELM losses based on the ratio of convective, $\tau_n \sim L_{||}/c_S$, and conductive, $\tau_T \sim L_{||}^2/\chi_e$, parallel loss times, e.g. it predicts mainly conductive losses at low ν^*, when the plasma cools faster than it rarefies ($\tau_n >> \tau_T$), and mainly convective losses at high ν^*, when cooling and rarefication are comparable ($\tau_n \sim \tau_T$), i.e. it explains why small (collisional) ELMs are mainly convective.

The model has been successful at reproducing a range of ELM filament measurements on JET, including the fraction of ELM energy deposited on the outer limiters (as measured by infra-red thermography, and also observed as energy missing from the divertor), which is typically ~10% for nominal Type-I ELMs [48]. Crucially, this fraction is found to decrease with ELM size, suggesting that smaller ELM filaments travel slower, i.e. have a lower radial Mach number, since for convective losses,

$$\frac{\lambda_W^{ELM}}{L_{||}} \approx \frac{V_\perp^{ELM}}{c_S} = M_\perp^{ELM}, \quad \frac{W_{wall}^{ELM}}{W_{tot}^{ELM}} \approx \exp\left(-\frac{0.5\Delta_{ped} + \Delta_{SOL}}{\lambda_W^{ELM}}\right) \tag{9}$$

where λ_W^{ELM} is the (SOL-averaged) decay length of ELM filament energy, and $W_{wall}^{ELM}/W_{tot}^{ELM}$ is the fraction of the ELM energy reaching the wall (note that $W_{tot}^{ELM} = \Delta W_{ELM}$). Interchange dynamics, which are expected to dominate the ELM filament motion, predict that $M_\perp$ should increase as the square-root of the perpendicular filament size and the relative pressure perturbation [16],

$$M_\perp^{int} = \frac{V_\perp^{int}}{c_S} = \left(\frac{2l}{R}\frac{\Delta p}{p_0}\right)^{1/2} \tag{10}$$

where l is the average perpendicular size of the filament, R is the major radius, Δp is the pressure perturbation due to the filament and p_0 is the background pressure. The relative pressure perturbation due the ELM filament remains roughly constant with ELM size, since $\Delta p/p_0 \sim p_{ped}/p_{sep} \sim const$. On the other hand, the perpendicular size of the filament may be related to the relative ELM amplitude, $\Delta W_{ELM}/W_{ped}$, as follows,

$$\frac{\Delta W_{ELM}}{W_{ped}} = \frac{\Delta V}{V} = \frac{2\pi\kappa a \Delta r}{\pi\kappa a^2} = 2\frac{\Delta r}{a},$$
$$\frac{W_{fil}}{W_{ped}} = \frac{V_{fil}}{V} = \frac{qa\kappa\Delta r\Delta\theta}{\pi\kappa a^2} = \frac{\Delta\phi}{\pi}\frac{\Delta r}{a} = \frac{2}{n_0}\frac{\Delta r}{a} \tag{11}$$

where $W_{ped} = 3/2 \times p_{ped}V$, $\Delta W_{ELM} = 3/2 \times p_{ped}\Delta V$, and $W_{fil} = 3/2 \times p_{ped}V_{fil}$ are the pedestal, ELM and ELM filament energies, respectively, V, ΔV and V_{fil} are the plasma, ELM-affected and filament volumes, Δr and a are the ELM-affected and plasma minor radii, $m_0 = 2\pi/\Delta\theta$ and $n_0 = 2\ \pi\ /\Delta\varphi$ are the initial poloidal and toroidal mode numbers of the ELM, $q = m_0/n_0$ is the safety factor and κ is the plasma elongation. Since the scaling (10) was derived for a circular, Gaussian filament shape, $\exp(-(\mathbf{x}/l)^2)$, one is justified in treating the size scaling as a free parameter, i.e.

$$l \approx l_\perp^\gamma l_\wedge^{1-\gamma} \approx (\Delta r)^\gamma (a\Delta\theta)^{1-\gamma}, \tag{12}$$

where $\gamma = 0$ corresponds to a purely poloidal dependence, which may be taken as the default Ansatz since the poloidal gradient is the main driving term. However, ELM filament heat loads on main chamber PFCs on JET [26] indicate that the number of filaments decreases roughly linearly with ELM size, $n_w \sim 3n_0 \sim 6/(\Delta W_{ELM}/W_{ped})$,

$$\frac{l_\perp}{a} \approx \frac{\Delta r}{a} \approx \frac{3}{n_w} \approx \frac{1}{n_0}, \quad \frac{l_\wedge}{a} \approx \frac{a\kappa\Delta\theta}{a} \approx \frac{2\pi\kappa}{n_0 q}, \quad \frac{l_\wedge}{l_\perp} \approx \frac{2\pi\kappa}{q} \approx 3 \tag{13}$$

so that the *initial* filament aspect ratio, $l_\wedge/l_\perp$, is independent of n_0 and hence of $\Delta W_{ELM}/W_{ped}$; a similar result, with $l_\wedge/l_\perp \sim 3$, was also obtained based on measurements of $l_\wedge$ and $l_\perp$ on several tokamaks [30]. It is interesting to note that the JET measurements indicate that this aspect ratio changes to $l_\wedge/l_\perp \sim 2\pi\kappa/3q \sim 1$ by the time the filaments make contact with the wall, i.e. the filaments change from being poloidally elongated to being roughly circular as they travel through the SOL, in agreement with simulations.

Combining the above results, one finds a general expression for the interchange scaling of the radial Mach number of ELM filaments,

$$M_{\perp}^{\mathrm{int}} \sim \left(\frac{2l_{\perp}^{\gamma} l_{\wedge}^{1-\gamma}}{a/\varepsilon}\right)^{1/2} \sim \left[2\varepsilon\left(\frac{2\pi}{q}\right)^{1-\gamma}\frac{1}{n_0}\right]^{1/2} \sim \left[\varepsilon\left(\frac{2\pi}{q}\right)^{1-\gamma}\frac{\Delta W_{ELM}}{W_{ped}}\right]^{1/2} \tag{14}$$

where $\varepsilon = a/R$; for default values $\gamma = \delta = 0$ this yields $M_{\perp}{}^{int} \sim (2\pi\varepsilon/q)^{1/2}(\Delta W_{ELM}/W_{ped})^{1/2}$. Note that the scaling with ELM amplitude is independent of γ, due to the observed constancy of the initial filament aspect ratio, (13). This prediction compares favourably with exponents inferred from measurements on JET using turbulence transport probes [59]: $M_{\perp}{}^{int} \sim (\Delta W_{ELM}/W_{ped})^{\alpha}$, $\alpha \sim 0.3$–0.4; the divertor energy deficit [12,28,29,48]: $\alpha \sim 0.3$–0.5; and direct infrared measurements of heat loads on the outboard limiters [47], $\alpha \sim 0.4$. These results suggest the interchange scaling (14) slightly overestimates the exponent α, unless the ratio of pedestal and separatrix pressures decreases weakly with ELM amplitude. More likely, sheath dissipative effects modify the interchange scaling with ELM amplitude, reducing α below 0.5. The predictions of $M_{\perp}{}^{int}$ increasing with ε and decreasing with q, are yet to be tested, although the former is consistent with results from MAST ($\varepsilon \sim 1$) in which higher $M_{\perp}{}^{int}$ are measured than in conventional tokamaks ($\varepsilon \sim 13$) [28,29].

The JET results may be used to predict the average ELM filament heat loads on the first wall in the reference ITER scenario (4 keV pedestal, $q_{95} \approx 3$). For given values of Δr and $\Delta W_{ELM}/W_{ped}$, the fraction of ELM energy to the wall on ITER may be approximated to lowest order using Eq. (9). Extrapolating directly from JET measurements, the perpendicular Mach number and the ELM filament energy width, $\lambda_W{}^{ELM} \approx L_{||} M_{\perp}{}^{ELM}$, may be estimated as

$$M_{\perp}^{ITER} \propto \left(\frac{3}{q_{95}}\right)^{\frac{1-\gamma}{2}}\left(\frac{\Delta W_{ELM}/W_{ped}}{0.12}\right)^{0.4}, \quad \lambda_W^{ELM.ITER}[cm] \approx 2 \times 2.5\left(\frac{3}{q_{95}}\right)^{\frac{1-\gamma}{2}}\left(\frac{\Delta W/W_{ped}}{0.12}\right)^{0.4} \tag{15}$$

which is a generalization of the expression suggested in [12]; in the above we used the JET value of $\lambda_W{}^{ELM} \sim 3$ cm obtained for $\Delta W/W_{ped} \sim 0.12$ and $q_{95} \approx 3$, as well as the fact that $L_{||} \sim q_{95}R$ is twice as large on ITER than on JET due to the larger major radius. The fraction of ELM energy reaching the wall in ITER may be predicted using two methods: (i) a simple exponential decay, combining Eqs. (9) and (15), and (ii) the parallel loss model with radial velocity scaled according to Eq. (15), i.e.

$$V_{\perp}^{ITER}[m/s] \approx 600\left(\frac{2}{0.8}\right)^{1/2}\left(\frac{3}{q_{95}}\right)^{\frac{1-\gamma}{2}}\left(\frac{\Delta W_{ELM}/W_{ped}}{0.12}\right)^{0.4}, \tag{16}$$

where the ratio inside the square-root reflects the temperatures at mid-pedestal conditions, 2 keV in ITER vs 800 eV in JET. Here we set $\Delta_{ped}/2 = 2.5$ cm, $\Delta_{SOL} = 5$ cm to the upper baffle and $\Delta_{SOL} = 15$ cm to the outer limiter. The former method predicts $W' \sim 23\%$ and 0.8% reaching the upper baffle for natural ($\Delta W_{ELM} = 20$ MJ, $W_{ped} = 150$ MJ, $\Delta W/W_{ped} \sim 13.3\%$) and mitigated ($\Delta W_{ELM} = 1$ MJ, $\Delta W/W_{ped} \sim 0.66\%$) ELMs, respectively, and $W' \sim 3\%$ and $\sim 10^{-5}$ reaching the outer limiter. The latter, more accurate method, also predicts $W' \sim 25\%$ for the natural ELMs, but a substantially higher value, $W' \sim 4\%$,or the mitigated ELMs at the outer baffle. On the basis of this analysis one may conclude that the maximum ELM size on ITER will be determined by the heat load limits on divertor PFCs, rather than main chamber PFCs.

3.5. ELM heat loads and impurities

How can one reduce the ELM heat loads on the divertor? Can most of the ELM energy be radiated in the divertor, before striking the targets? Unfortunately, the answer is no. It has now been demonstrated, beyond reasonable doubt, that such 'buffering' of the ELM energy by the divertor can at most remove a small fraction (~10–20%) of the energy released during a typical, Type-I ELM. Indeed, such buffering is only observed for small ELMs (below 20 kJ on JET), with the findings explained by EDGE2D/NIMBUS simulations in terms the limited amount of energy that can be radiated in the divertor on the time scale of the ELM [39,42,72]. One may hope that divertor detachment would facilitate such 'buffering' but again this would be false. The ELM heat pulse effectively 'burns through' the neutral gas buffer and transiently reattaches the plasma, so that under Type-I H-mode conditions, detachment is only maintained during the inter-ELM phase (this is not true for the small, Type-III ELMs whose size is below the 'buffering' threshold). Here care should be taken not to mistake the radiation spike often observed after the ELM (which can be comparable to the energy released by the ELM) with any radiative buffering of the ELM energy [21,49]. The former is simply a consequence of the influx of impurities released from the targets by the ELM plasma load. Rather than providing a beneficial effect, this radiation spike can lead to strong cooling of the X-point region, which for sufficiently large ELMs, can cause a back transition to the L-mode regime.

The problem of ELM induced impurity inflows is particularly acute for tungsten PFCs, since the ELM pulse is characterized by hot ions (at keV energies), including any impurity ions present in the pedestal region, which can lead to significant physical sputtering of the W tiles. This process has been recently observed at AUG, where the inter-ELM W influx from the outer divertor is strongly reduced as divertor plasma is cooled below ~10 eV [6,44]. With the outer divertor detached, the average W influx is dominated by ELMs and the transient W influx increases with ELM energy. Significantly, both the inter-ELM and ELM influxes are dominated by impurity sputtering. It was found that Argon seeding decreased erosion between ELMs (by cooling the plasma below the threshold temperature) but increased W erosion during ELMs (since the ELM ions were always energetic enough to sputter W atoms). The optimum seeding rate (smallest W influx) is thus determined by competition between erosion by Ar ions and cooling by Ar radiation.

3.6. ELM size/frequency control techniques

Is there then no way to reduce the ELM heat load by means of radiative impurities? We have already touched on the answer in the form of the Type-III ELMs, which represent one of the three leading methods to significantly reduce the ELM size, the others being pellet injection and magnetic field perturbation. It is worth noting that many other small ELM regimes have been discovered in tokamak experiments, e.g. grassy ELMs in JT-60U and AUG, Quiescent H-mode in DIII-D and JT-60U, and Type-II ELMs in AUG; on JET, such small ELM regimes have only been observed at either relatively high q_{95} values ($q_{95} > 5$), or in quasi-double null configurations [55], making them irrelevant to the baseline ITER scenario for which $q_{95} \sim 3$ (although not to the AT scenario, for which $q_{95} \sim 5$). It has been know for a long time that the ELM frequency can be increased (and the ELM size reduced) substantially, i.e. by a factor of greater than 10, by cooling the pedestal plasma and thus affecting a transition from Type-I, to Type-III, ELMs. Whereas Type-I ELM stability boundary is determined by ideal MHD (peeling-ballooning) modes, Type-III ELMs are ideal-MHD stable and are thus controlled by resistive-MHD (this explains why the condition for the I-III transition has been linked to the critical pedestal temperature and hence resistivity) [2]. At presented, Type-III ELMy H-mode is the only scenario which has been demonstrated to be compatible with all ITER exhaust requirements ($f_{rad} \sim 75\%$, $f_{GW} \sim 0.85$, $q_{95} \sim 3$, $Z_{eff} < 2$, outer divertor detachment, and most notably, $\Delta W/W_{ped} < 0.01$)[72], although at a 'penalty' of a ~50% drop in pedestal pressure/temperature and hence a ~15–20% drop in H_{98}. If applied to ITER this solution would clearly have an adverse effect

on the fusion gain, Eq. (3), with the reduction variously estimated as between ~30% and ~50% [68,72]. It should be noted however that $Q \sim 10$ could be recovered were it possible to increase the plasma current from 15 to 17 MA (i.e. by 15%).

The second method of reducing the ELM size consists of increasing the Type-I ELM frequency by injection of small deuterium ice pellets at a frequency at least 50% greater than the natural ELM frequency. As the pellet ablates in the edge region it provides a perturbation which triggers some type of instability. The strength of this trigger appears to be correlated only to the penetration depth of the pellet. As a result, provided the pellet is sufficiently large, it can trigger a Type-I ELM at any point in the ELM cycle! This technique, known as *pellet ELM pacing*, has been extensively tested in AUG, where f_{ELM} has been increased by up to a factor of 2, albeit at the reduction of the plasma stored energy and energy confinement, H_{98}, by roughly ~10–20%. However, this reduction, which stems from increased convective losses, i.e. from the additional plasma fuelling provided by the pellets, simply indicates that the pellets used were too large for the task, i.e. that the effects of plasma fuelling and ELM pacing could not be decoupled on AUG. This issue should be addressed shortly in the planned experiments on JET, where the two effects of fuelling and pacing become easier to decouple. Nonetheless, there are two major questions to be resolved regarding this ELM control technique, namely: can pellet ELM pacing be demonstrated near $f_{GW} \sim 0.85$? and can pellet injection produce a strong enough perturbation on ITER to trigger an edge instability (Type-I ELM) without triggering a core instability (e.g. a neoclassical tearing mode)?

The final technique of controlling the ELM size, and indeed, under certain conditions of suppressing ELMs altogether, consists of distorting, and to a large extent ergodizing, the edge magnetic field by a resonant magnetic perturbation (RMP) via a parametric resonance [41]. This method, which has been developed primarily on DIII-D with a toroidal mode number of $n = 3$ [9], works most effectively with in-vessel coils, containing a significant poloidal harmonic, which ensures that the RMP is localized to the edge region. One of the hallmarks of RMP, and the associated magnetic ergodization, is the reduction of the edge plasma density due to increased parallel losses to the divertor targets. This effect, known as 'magnetic pump-out', was first observed with ergodic divertors, e.g. Tore-Supra [18]. Significantly, and somewhat surprisingly, it represents edge plasma rarefication (Δn), but not cooling (ΔT), i.e. the edge temperature remains roughly constant! As a result the pedestal density and pressure are reduced by ~15–30%, while the energy confinement is roughly preserved, albeit in relatively low density plasmas [10]. However, it remains to be seen whether this density drop can be recovered (to the required level of $f_{GW} \sim 0.85$) by increased particle fuelling, either by gas puffing or pellet injection, without loss in energy confinement, i.e. an effective reduction of W_{ped} or H_{98} due to the edge cooling associated with increased re-fuelling (here the experience with the ergodic divertor in T–S, and with EFCC and toroidal field ripple (TFR) experiments on JET, see below, suggests otherwise). Finally, it is not clear whether ELM suppression could be maintained in the presence of pellet fuelling (as required for ITER), since large, 'fuelling' pellets generally trigger an ELM anywhere in the ELM cycle, even when the pedestal pressure gradient is ideal MHD stable. Nonetheless, RMPs offer a very promising technique of controlling edge pressure gradients and ELM behaviour in tokamaks, although clearly more experiments are needed to answer the above questions.

Similarly, a significant reduction of the ELM size (increase of ELM frequency) has also been observed with external perturbations to the toroidal field. These include both low ($n = 1,2$) and high ($n = 16$) toroidal mode numbers, the former generated with error field correction coils (EFCCs) [34], the latter by varying the TFR [56], e.g. when the ripple was increased from 0.1% to 1% in JET, the relative ELM size, for a given pedestal collisionality, was reduced by a factor of 2 (this change was related to smaller conductive losses, i.e. mainly convective ELMs, and was much less pronounced at higher density, i.e. for $f_{GW} \sim 0.85$). With both techniques, the pedestal density and pressure was reduced due to, what appears to be, a 'magnetic pump-out' effect. In the case of TFR, which is inherent in any tokamak and is expected to have a nominal value at the outer mid plane of ~0.3% in ITER (compared with ~0.08% on JET), this loss of pedestal pressure was not recovered by increased fuelling, which merely led to increased cooling of the pedestal and so a reduction of H_{98}. Similar results were found in the case of EFCC [25], with the maximum achievable density reduced from $f_{GW} \sim 0.95$ to ~0.8 and H98 reduced by 10–20%.

One possible explanation of the above effects has emerged from recent investigations on JT-60U, which reveal a strong correlation between toroidal plasma rotation and the ELM size [46], suggesting that the latter could be modified by varying the former, e.g. by braking the plasma by non-axisymmetric external fields. However, it is not clear to what extent this technique is applicable in a burning plasma where the bulk of the plasma rotation is likely to be spontaneously generated.

The various ELM control techniques are summarised and compared in Table 1 which lists the best results obtained so far in terms of f_{ELM}, f_{GW} and H_{98}.

4. Conclusions

We have seen that 'integration' and 'compatibility' of plasma scenarios and PFCs, is not a binary signifier, but a qualitative one, and amounts to the optimization of the former (subject to the latter) with respect to the fusion gain factor Q, thus determining the maximum Q for a given reactor design. Put another way, the boundary plasma conditions (e.g. PFC limits) determine the maximum fusion gain. One can quantify the 'cost' of these PFC limits in terms of the relative reduction in Q with respect to the unconstrained value, e.g. if arbitrarily high steady-state and transient heat loads on divertor and main chamber PFCs were permitted.

Table 1
Summary of ELM control techniques, comparing the best results achieved so far in terms of preserving density and energy confinement (asterix '*' indicates that the technique has not been fully optimized). The values are indicative only and represent a compromise between the f_{GW} and H_{98}, towards matching the values required by ITER ($f_{GW} \sim 0.85$, $H_{98} \sim 1$).

Method (machine)	Increase in f_{ELM} vs Type-I ELM frequency	Density confinement, f_{GW}, and (% reduction)	Energy confinement, H_{98}, and (% reduction)	Issues and problems
Type-III (JET)	×30	~0.85* (0%)	~0.85* (~15%)	Energy confinement
Pellet pacing (AUG)	×2*	~0.5*	~0.8* (20%)	Decoupling from fuelling
RMPs (DIIID)	Complete suppression	~0.25*	~1 (~15–30% in p_{ped})	Density confinement
RMPs (DIIID)	×20	~0.6*	~0.9* (~0% in p_{ped})	Energy confinement
EFCC (JET)	×10	~0.78* (~10%)	~ 0.85* (~15%)	Density confinement
TFR (ripple) (JET, JT60U)	×2	~0.8* (~5%)	~0.85* (~15%)	Density and energy conf.
Magnetic pacing (JET)	×30	~0.5*	~0.85* (~15%)	Magnetic shielding

On the basis of our present knowledge (experiment) and understanding (theory) of the plasma exhaust processes, it appears that this cost, $\zeta = \Delta Q/Q_0$, Eq. (3), is negligible for existing tokamaks with Carbon PFCs, in which PFC limits are rarely reached and impurity seeding is not a necessary condition, but could be significant (of order ~30–50% or more) for ITER and DEMO with metal PFCs. The dominant contribution to this reduction is the requirement of small ELMs ($\Delta W/W_{ped} < 1\%$), which entails a reduction of the pedestal pressure by ~30–50% and of the energy confinement by ~10–15%. Although active ELM control by pellet injection and magnetic perturbations hold much promise and are a topic of intense research in tokamak programs worldwide, it remains to be seen whether these methods offer a smaller performance cost, ζ, than the more conventional method of Type-III ELMy H-mode. At the moment, the latter appears to be the only plasma scenario compatible with all ITER exhaust criteria, including the heat load limits on PFCs. Indeed, since significant radiative impurity seeding is necessary in ITER to ensure detached divertor operation (in order to minimize W sputtering), and the exact mechanism governing the Type-I to Type-III transition is poorly understood, one may yet find that the transition to Type-III ELMy H-mode becomes unavoidable in ITER at the levels of radiation ($f_{rad} > 75\%$) required by the steady-state PFC limit of 10 MW/m^2. Finally, and perhaps most worryingly of all, is the unknown effect of the large transient W influxes after the ELM, on the edge transport barrier and ELM dynamics – a process which could become self-limiting if the W inflow destroys the ETB by affecting an H to L back transition. Indeed, the very access and maintenance of the H-mode appears problematic, as the required $P_{SOL}/P_{LH} \sim 2$ may exceed the steady-state PFC limit if sufficient energy (>50%) cannot be radiated in the divertor volume.

The above issues clearly cannot be resolved without continued experimental and theoretical investigations. On the experimental front, tokamak operation with metal walls as in Alcator C-mod (Mo), AUG (W) and the upcoming JET ITER-like wall (Be,W) is highly valuable. On the theoretical front, an essential tool are intergrated simulations linking the three tokamak regions (core, edge, SOL) with PFC elements, which must be compared and benchmarked against experimental data to offer predictive capability for ITER. Moreover, it would be highly desirable to further benchmark these tools in the hydrogen phase of ITER, i.e. before the nuclear phase of the experiment, and to extrapolate to the deuterium phase based on modelling of hydrogen and deuterium plasmas in existing tokamaks.

Acknowledgements

I would like to thank the many contributors to this review, specifically A. Alonso, G. Arnoux, R. Dux, P. deVries, T. Eich, T.Evans, M.Fenstermacher, A. Huber, S. Jachmich, M. Jakubowski, E.Joffrin, A. Kirk, T. Loarer, B.LaBombard, P.Lang, Y.Liang, B. Lipschultz, A. Loarte, G. F. Matthews, D. Moulton, V. Naulin, R. Neu, R.A. Pitts, J. Rapp, F.Sartori, G.Saibene, D. Tskhakaya, M. Wischmeier and many JET EFDA Contributors. The work was funded jointly by the UK Engineering and Physical Sciences Research Council and by the European Communities under the contract of Association between EURATOM and UKAEA. The view and opinions expressed herein do not necessarily reflect those of the European Commission.

References

[1] G. Arnoux et al., J. Nucl. Mater. 390–391 (2009) 263.
[2] M. Beurskens et al., Nucl. Fus. (2008).
[3] J. Boedo et al., J. Nucl. Mater. 390–391 (2009) 29.
[4] J.W. Connor, H.R. Wilson, Plasma Phys. Control. Fus. 42 (1) (2000) R1.
[5] A.V. Chankin et al., Nucl. Fus. 47 (5) (2007) 479.
[6] R. Dux et al., J. Nucl. Mater. 390–391 (2009) 858.
[7] W. Eckstein, V. Philipps, in: W. Hofer, J. Roth (Eds.), Physical Processes of the Interaction of Fusion Plasmas with Solids, Academic Press, San Diego, 1996.
[8] T. Eich et al., J. Nucl. Mater. 363–365 (2007) 989;
T. Eich et al., J. Nucl. Mater. 390–391 (2009) 760.
[9] T. Evans et al., Nucl. Fus. 48 (2) (2008) 024002. p. 10;
T. Evans et al., Phys. Plasmas 13 (2006) 056121.
[10] M.E. Fenstermacher et al., Phys. Plasmas 15 (2008) 056122.
[11] W. Fundamenski, R.A. Pitts, Plasma Phys. Control. Fus. 48 (2006) 109.
[12] W. Fundamenski et al., J. Nucl. Mater. 363–365 (2007) 319.
[13] W. Fundamenski et al., Plasma Phys. Control. Fus. 49 (5) (2007) R43.
[14] W. Fundamenski et al., Nucl. Fus. 47 (5) (2007) 417.
[15] X. Garbet et al., Plasma Phys. Control. Fus. 47 (6) (2005) 957;
X. Garbet et al., Plasma Phys. Control. Fus. 46 (9) (2004) 1351.
[16] O.E. Garcia et al., Phys. Plasmas 13 (2006) 082309.
[17] O.E. Garcia et al., Plasma Phys. Control. Fus. 49 (12B) (2007) B47;
O.E. Garcia et al., Plasma Phys. Control. Fus. 48 (1) (2006) L1.
[18] Ph. Ghendrih et al., Plasma Phys. Control. Fus. 38 (10) (1996) 1653;
Ph. Ghendrih et al., Plasma Phys. Control. Fus. 39 (12B) (1997) B207.
[19] C. Giroud et al., Nucl. Fus. 47 (4) (2007) 313.
[20] M.J. Greenwald, Plasma Phys. Control. Fus. 44 (8) (2002) R27.
[21] A. Huber et al, this conference:;
A. Huber et al., Nucl. Fus. (2007).
[22] ITER Physics Expert Group on Divertor, ITER Physics Expert Group on Divertor Modelling and Database and ITER Physics Basis Editors, Nucl. Fus. 39 (12) (1999) 2391.
[23] A. Loarte et al., Nucl. Fus. 47 (6) (2007) S203.
[24] E.J. Doyle et al., Nucl. Fus. 47 (6) (2007) S18.
[25] S. Jachmich et al., J. Nucl. Mater. 390–391 (2009) 768.
[26] M. Jakubowski et al., this conference.
[27] K. Kamiya et al., Plasma Phys. Control. Fus. 49 (7) (2007) S43.
[28] A. Kirk et al., J. Nucl. Mater. 390–391 (2009) 727.
[29] A. Kirk et al., Plasma Phys. Control. Fus. 48 (12B) (2006) B433.
[30] A. Kirk et al., Plasma Phys. Control. Fus. 49 (8) (2007) 1259.
[31] G. Kirnev et al., Plasma Phys. Control. Fus. 49 (6) (2007) 689.
[32] B. LaBombard et al., Nucl. Fus. 40 (12) (2000) 2041;
B. LaBombard et al., Nucl. Fus. 44 (10) (2004) 1047.
[33] A. Leonard et al., Plasma Phys. Control. Fus. 48 (5A) (2006) A149.
[34] Y. Liang et al., this conference:;
Y. Liang et al., Plasma Phys. Control. Fus. 49 (12B) (2007) B581.
[35] J. Linke et al., J. Nucl. Mater. 367 (August) (2007) 1422.
[36] B. Lipschultz et al., Nucl. Fus. 47 (9) (2007) 1189.
[37] T. Loarer et al., this conference, paper R-3.
[38] A. Loarte et al., Phys. Plasmas 11 (2004) 2668;
A. Loarte et al., Plasma Phys. Control. Fus. 45 (9) (2003) 1549;
A. Loarte et al., Plasma Phys. Control. Fus. 44 (9) (2002) 1815.
[39] G.P. Maddison et al., Nucl. Fus. 43 (1) (2003) 49.
[40] G.F. Matthews et al., Nucl. Fus. 39 (1) (1999) 19.
[41] R. Moyer et al., this conference.
[42] P. Monier-Garbet et al., Nucl. Fus. 45 (11) (2005) 1404.
[43] V. Naulin et al., J. Nucl. Mater. 363–365 (2007) 24.
[44] R. Neu et al., J. Phys.: Conf. Ser. 100 (2008) 062001.
[45] N. Oyama et al., Plasma Phys. Control. Fus. 48 (5A) (2006) A171.
[46] N. Oyama07 et al., Plasma Phys. Control. Fus. 49 (2007) 249.
[47] R.A. Pitts et al., J. Nucl. Mater. 390–391 (2009) 755.
[48] R.A. Pitts et al., Nucl. Fus. 46 (2006) 82.
[49] R.A. Pitts et al., Plasma Phys. Control. Fus. 47 (12B) (2005) B303.
[50] T.D. Rognlien, D.D. Ryutov, Contribution Plasma Phys. 38 (1998) 152.
[51] J. Roth et al., J. Nucl. Mater. 390–391 (2009) 1.
[52] G.J. Radford et al., Contribution Plasma Phys. 36 (1996) 187;
A.V. Chankin et al., Contribution Plasma Phys. 40 (2000) 288.
[53] J. Rapp et al., Nucl. Fus. 44 (2) (2004) 312.
[54] J. Rapp et al., J. Nucl. Mater. 337–339 (2005) 826.
[55] G. Saibene et al., Nucl. Fus. 45 (2005) 297.
[56] G. Saibene et al., Nucl. Fus. 47 (2007) 969.
[57] R. Schneider et al., J. Nucl. Mater. 266–269 (1999) 175;
V. Rozhansky et al., Nucl. Fus. 41 (2001) 387.
[58] B. Scott, Plasma Phys. Control. Fus. 49 (7) (2007) S25;
B. Scott, Plasma Phys. Control. Fus. 48 (12B) (2006) B277.
[59] C. Silva, private communication.
[60] P. Stangeby, Plasma Boundary of Magnetic Fusion Devices, IoP Press, Bristol, 2000.
[61] J.D. Strachan et al., Nucl. Fus. 44 (7) (2004) 772.
[62] H. Takenaga et al., Nucl. Fus. 43 (2003) 1235.
[63] G. Telesca et al., Nucl. Fus. 36 (3) (1996) 347.
[64] G. Telesca et al., Nucl. Fus. 47 (11) (2007) 1625.
[65] D. Tskhakaya et al., Contribution Plasma Phys. 48 (2008) 89.
[66] D. Tskhakaya et al., J. Nucl. Mater. 390–391 (2009) 335.
[67] M. Wischmeier et al., J. Nucl. Mater. 390–391 (2009) 250.
[68] R. Zagorski et al., Contribution Plasma Phys. 48 (2008) 179;
R. Zagorski et al., J. Nucl. Mater. 390–391 (2009) 404.
[69] A. Zhitlukhin et al., J. Nucl. Mater. 363–365 (2007) 301.
[70] S.J. Zweben, Plasma Phys. Control. Fus. 49 (7) (2007) S1.
[71] W. Fundamenski, Plasma Phys. Control. Fus. 47 (2005) R163.
[72] J. Rapp et al., J. Nucl. Mater. 390–391 (2009) 238.